Solar Energy Materials & Solar Cells 94 (2010) 1118–1124

Contents lists available at ScienceDirect

Solar Energy Materials & Solar Cells

journal homepage: www.elsevier.com/locate/solmat

Optimization of thickness and morphology of active layer for high performance of bulk-heterojunction organic solar cells

Young Min Nam [a], June Huh [b], Won Ho Jo [a,*]

[a] Department of Materials Science and Engineering, Seoul National University, Seoul 151-742, Republic of Korea
[b] Department of Materials Science and Engineering, Yonsei University, Seoul 120-740, Republic of Korea

ARTICLE INFO

Article history:
Received 11 December 2009
Received in revised form
23 February 2010
Accepted 25 February 2010
Available online 20 March 2010

Keywords:
Drift-diffusion model
Transfer matrix formalism
Bulk-heterojunction
Organic solar cell
P3HT:PCBM.

ABSTRACT

A two-dimensional model accounting for the effect of both the morphology of active layer and the layer configuration of multilayer-structured device on the device performance, is developed to optimize the device parameter for high performance of the bulk-heterojunction organic solar cells. When the photovoltaic properties of poly(3-hexylthiophene)/[6,6]-phenyl C61-butyric acid methyl ester solar cells are calculated as functions of device parameters by using the model, it is found that the optimum thickness of active layer is 80 nm and that the domain size in active layer is about 6 nm. Comparison of simulation with experiment reveals that the simulated short-circuit current as a function of active layer thickness is very consistent with experimental one.

1. Introduction

Organic photovoltaic cells (OPVs) have received much attention as a promising alternative to silicon based solar cells due to the low-cost power generation and easy processability [1–6]. The performance of polymer solar cells has been greatly improved by introduction of bulk-heterojunction (BHJ) concept for an active layer where electron donor and acceptor materials [7–12], the most common choice being poly(3-hexylthiophene) (P3HT) and [6,6]-phenyl C61-butyric acid methyl ester (PCBM), are mixed in solution and cast into a thin film sandwiched between two electrodes [13–16]. Recently, much efforts have been devoted to improve the performance of BHJ OPVs by enhancing light absorption [17,18] or controlling the domain size [16,19,20]. However, despite recent improvement, the efficiencies of organic BHJ devices are not yet high enough to be commercially viable [21,22]. Furthermore, some other issues such as large area processing [1,23–25] and stability [26,27] are also important for commercialization.

The basic operation principle of BHJ device is rather simple, relying largely on the characteristics of phase-separated structure in the active layer consisting of electron donor and acceptor components. The light incident upon the BHJ active layer where donor and acceptor components are segregated into phase-separated domains gives rise to formation of excitons that must diffuse to the donor–acceptor interface, where the subsequent event of electron–hole charge separation occurs [2,28]. Subsequently, the dissociated electrons and holes move through the percolated domains toward their corresponding electrodes, ultimately accomplishing the power conversion from solar energy into electric energy [28]. The morphology of the active layer is a critical factor to be optimized for the BHJ device performance [11,29–32]. For instance, large domains in the phase-separated structure will prevent efficient charge separation, whereas small domains will result in a poorly percolated domain structure and thereby increase the possibility of charge carrier recombination [32]. The thickness of active layer is also an important factor that affects absorption of light and thus exciton generation inside the active layer [33–35]. Since a BHJ device is made of a number of layers stacked sequentially on top of each other, the optical events such as reflections at interfaces between layers and their interferences pose a complex optimization task with respect to the thickness of active layer, where the light source going through all the optical effects should be maximally collected.

Several theoretical or numerical studies have been performed to correlate the photovoltaic properties with the morphology of the active layer in OPV [33–49]. Most notably, the drift-diffusion model, which is based on a series of self-consistent equations for the electrostatic potential and the densities of electron, hole and exciton, can predict a time-evolution of current distributions and *J–V* curves, provided that the morphology of active layer and its material parameters are given. As an earlier effort, Barker et al. [48] developed a drift-diffusion model for OPVs to capture one-dimensional device physics of a bilayer system and obtained

* Corresponding author. Tel.: +82 2 880 7192; fax: +82 2 885 1748.
E-mail address: whjpoly@snu.ac.kr (W. Ho Jo).

0927-0248/$ - see front matter © 2010 Elsevier B.V. All rights reserved.
doi:10.1016/j.solmat.2010.02.041

good agreement with experimental data. However, they simulated the generation of electrons and holes at the interface by assuming that only some fraction of light source leads to charge separation, instead of explicitly considering the spatial distribution of excitons. Koster et al. [49] have also developed a one-dimensional drift-diffusion model for polymer:fullerene BHJ OPVs, where the device is considered to consist of a single semiconductor material. However, because such one-dimensional drift-diffusion model can be applicable only to a homogeneous or bilayer system described by one-dimensional density fluctuation across the active layer, an extension of drift-diffusion model to higher dimension is inevitable in order to account for the effect of morphological structure. Recently, Buxton and Clark [37,38] have developed the drift-diffusion model in two-dimension to simulate charge generation process in a phase-separated system consisting of donor and acceptor phases, which allows them to study the morphological effects such as domain size, order and percolation. Furthermore, the model is not merely an extension to two-dimensional case but also account for generation, diffusion, or dissociation of excitons in a more explicit way. However, the photogeneration of excitons in their model, which is treated by a simple function of exponential decay with the distance from the top of layer, neglects the possibility of light reflections and interferences caused by the presence of other layers (e.g., indium–tin-oxide (ITO), Al, etc.) above or below the active layer. These optical events due to multilayer structure of OPV affect significantly the efficiency of exciton generation. Therefore, a complete model taking into account all the aforementioned factors is necessitated for studying the correlation between the device parameters and the performance of the BHJ solar cell. Some optical reflection/interference models have been previously used for computing the distribution of optical electric fields in the multilayer structure and photovoltaic properties such as the current collection efficiency have been predicted under an oversimplified assumption that all generated excitons contribute to the short-circuit photocurrent [34–36,39,50–52].

In this report, as a more mature approach for photocurrent generation process in the BHJ device, we present a new approach combining the drift-diffusion model and the optical reflection/interference model in order to investigate the relationship between the structural variables and the performance of BHJ solar cell with active layer consisting of P3HT and PCBM.

2. Simulation method

2.1. Optical model

The optical model for multilayer structures in this study is based on the transfer matrix formalism (TMF) with two subsets of 2×2 matrices (layer and interface matrix), which has first been developed by Petterson et al. [33]. Since this approach has already been explained in great detail elsewhere [33,34,53], it is briefly described in this section.

As an input to the optical model, the thickness of each layer in the device is chosen from the common multilayer structure of P3HT:PCBM based solar cells: glass (1 mm)/SiO_2 (10 nm)/ITO (150 nm)/poly(3,4-ethylenedioxythiophene):polystyrenesulfonate (PEDOT:PSS) (50 nm)/P3HT:PCBM (d_{active})/LiF (1 nm)/Al (100 nm). As another input to the optical model, the complex refractive index ($\tilde{n}$) of each layer was measured or taken from the literature value. The complex refractive indices ($\tilde{n}$) of PEDOT:PSS and P3HT:PCBM (1:1) were measured by using multiangle ellipsometer and fitting software (EllyReg), which were almost the same as the data from literatures [39,54]. The data for other layers are taken from several sources [55–57]. The refractive index (n) and the extinction coefficient (κ) of each layer, as plotted against the wavelength (λ) in Fig. 1, will be used for optical simulation.

2.2. Drift-diffusion model

The drift-diffusion model consists of a Poisson's equation for the electrostatic potential (Ψ) and self-consistent equations for densities of electron (N), hole (P) and exciton (X), which accounts for the flux due to drift and diffusion at position z, the exciton generation rate (G), the exciton dissociation rate (D) and recombination rate (R) [37,38].

The rates of three events, the exciton generation, the dissociation of exciton and the hole–electron recombination, are given as follows: the exciton generation rate per unit volume $G(\mathbf{r})$ at position $\mathbf{r}=(x,z)$ is determined from the optical model described in the previous section by

$$G(\mathbf{r}) = \int_{\lambda_1}^{\lambda_2} \frac{\lambda}{hc} Q(z,\lambda)\, d\lambda, \tag{1}$$

where h is Planck's constant and c is the speed of light and the $Q(z,\lambda)$ is the time average of the energy dissipation per unit time

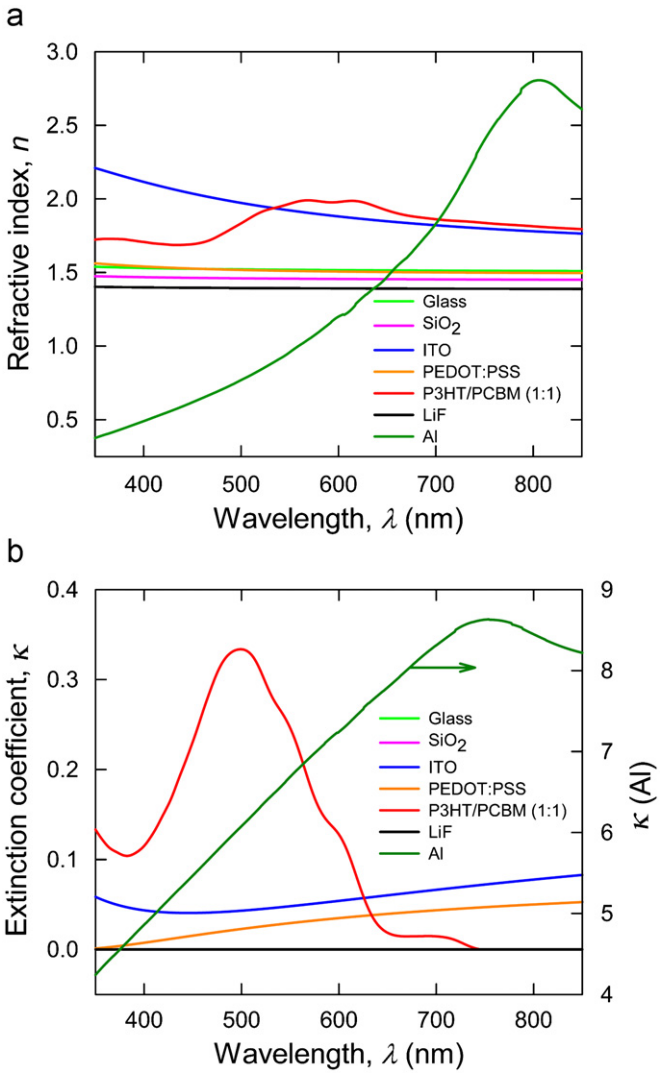

Fig. 1. The optical constants of materials used in simulation: (a) refractive indices n, (b) extinction coefficients κ. The data for SiO_2 and LiF are taken from Ref. [55], and the data for ITO and Al are taken from Refs. [56] and [57], respectively. The weight ratio of P3HT–PCBM is 1:1.

at the position z for the wave with λ [34,51]. For the active layer consisting of P3HT/PCBM, the integration limit is chosen as $\lambda_1=350$ nm and $\lambda_2=850$ nm because the transmission of glass below 350 nm and the absorption of P3HT/PCBM above 850 nm are negligibly small. The dissociation rate of exciton (D) is described by the Onsager–Braun theory [58, 59] and the recombination rate (R) is expressed by a bimolecular recombination of the Langevin form, which is given as $R(N,P)=q(\mu_N+\mu_P)NP/\varepsilon$ [45].

It should be noted that the drift-diffusion process does not take into account the molecular energy level of donor and acceptor phase and relies only on the gradients of electric field and density as the driving force responsible for the transport of charge carriers. Since the molecular energy levels are uneven around the donor–acceptor interface, the transport of holes (electrons) from one phase to another is affected by the energy difference of HOMOs (LUMOs) of donor and acceptor. For the purpose of modeling this, we follow a scheme proposed by Ruhstaller et al. [44]. This scheme introduces a stochastic weight of a species (hole or electron) hopping from α- to β-phase (α, β=donor/acceptor), $p_0=\min\{1,\exp[-(E_\beta-E_\alpha)/k_BT]\}$, where E_α is the HOMO (or LUMO) energy level of α-component for holes (or electrons), which therefore makes species diffuse preferentially through its corresponding phase.

For the current at the interface between the electrode and active layer, the boundary condition introduced by Scott and Malliaras [45] is adopted. The electrostatic potential at the boundary is obtained from the difference between the external voltage V_{appl} applied on the device and the built-in voltage V_{bi}: $\Psi(x,z=d_{active})-\Psi(x,z=0)=V_{bi}-V_{appl}$ where d_{active} is the thickness of the active layer. The built-in potential of the device is assumed to equal the difference between work functions of the two electrodes. Numerical solution of the equations is obtained by using the Scharfetter–Gummel method in the discretized two-dimensional space [60] with a given set of parameters and constants characterizing P3HT/PCBM BHJ. Parameters and constants used in this simulation are listed in Tables 1 and 2.

Table 1
Parameters used in drift-diffusion model.

Parameter	Symbol	Value
Zero-field hole mobility[a]	$\mu_{P,0}$	3.0×10^{-8} m^2 V^{-1} s^{-1}
Zero-field electron mobility[b]	$\mu_{N,0}$	3.0×10^{-7} m^2 V^{-1} s^{-1}
Field-dependent mobility parameter (hole)[a]	γ_P	2.4×10^{-4} m$^{1/2}$ V$^{-1/2}$
Field-dependent mobility parameter (electron)[b]	γ_N	1.1×10^{-4} m$^{1/2}$ V$^{-1/2}$
Exciton lifetime[c]	τ_X	400 ps
Exciton mobility[d]	μ_X	6.98×10^{-6} m^2 V^{-1} s^{-1}

[a] Space charge limited current (SCLC) hole mobility of P3HT. The value is taken from Ref. [63].
[b] SCLC electron mobility of PCBM. The value is taken from Ref. [64].
[c] Exciton lifetime is taken from Ref. [62].
[d] Exciton mobility is calculated from a diffusion length of 8.5 nm and a lifetime of 400 ps [62].

Table 2
Energy levels used in simulations.[a]

Energy level	Value (eV)
P3HT HOMO	5.2
P3HT LUMO	3.53
PCBM HOMO	6.1
PCBM LUMO	3.75
PEDOT:PSS work function	5.0
ITO work function	4.7
LiF/Al work function[b]	3.5

[a] The values are used from Ref. [65] except for LiF/Al.
[b] The value is given by Ref. [40].

3. Results and discussion

The complex refractive indices were measured from ellipsometer or taken from literatures [55–57]. When the measured optical parameters of materials for solar cells are plotted as a function of wavelength, as shown in Fig. 1, it reveals that the measured values are in good agreement with the data from literatures [39,57]. With these optical parameters, the number of photons absorbed in the active layer under AM 1.5 G condition [61] is calculated as a function of thickness of the active layer, as shown in Fig. 2. Since the extinction coefficient of PEDOT:PSS is much larger than other materials except P3HT:PCBM and electrodes, the photon absorption of the active layer is the highest when PEDOT:PSS is not used. However, since it is generally known that the PEDOT:PSS layer improves the hole transport from the active layer to anode, the PEDOT:PSS layer is commonly introduced in OPV. In this study, the PEDOT:PSS layer with thickness of 50 nm is used for simulation, because the thickness of 50 nm of PEDOT:PSS has been most commonly used and because the thickness variation of PEDOT:PSS from 30 to 50 nm does not give significant effect on the photon absorption in the active layer, as shown in Fig. 2. Fig. 2 also shows that the photon absorption has several peaks in the plot of absorbed photons versus the thickness of active layer. It has well been known that the behavior is induced by the interference between incident and reflected light from Al electrode: the peaks at around 80 and 220 nm in absorption of photons are attributed to strong constructive interference, which is in good agreement with previous reports [35,36].

To investigate the relationship between the performance of OPV and the internal structure of active layer, two-dimensional (2D) model for the morphology of active layer is used in this study, as shown in Fig. 3. Our 2D model assumes that the morphology representing BHJ is sinusoidal with two structural parameters, thickness of active layer (d_{active}) and the domain size (l_D), although the model does not represent accurately the

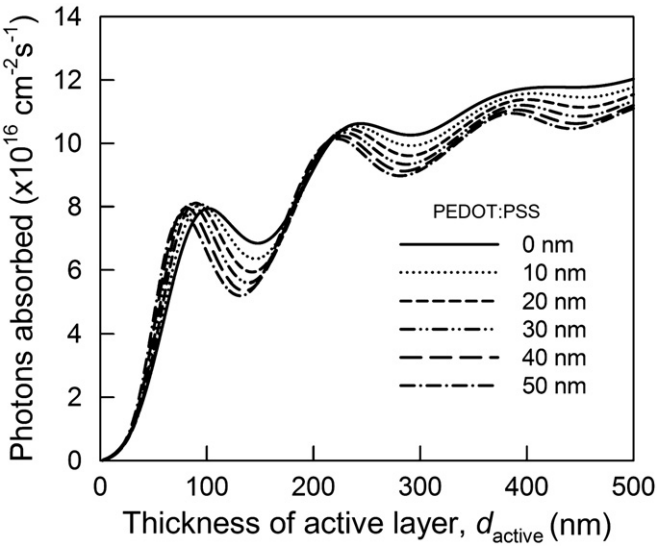

Fig. 2. Calculated photons absorbed in the P3HT:PCBM layer versus the thickness of active layer with different thickness of PEDOT:PSS: 0 nm (solid), 10 nm (dotted), 20 nm (short-dash), 30 nm (dash-dot-dot), 40 nm (long-dash) and 50 nm (dash-dot).

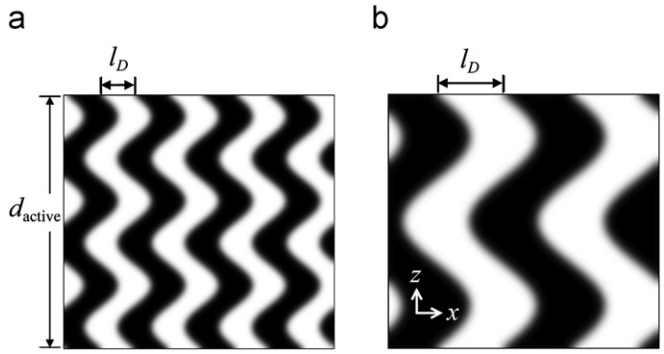

Fig. 3. Model morphologies for active layer of bulk-heterojunction organic solar cells with different domain size. The thickness of active layer and the domain size are denoted as d_{active} and l_D, respectively. White and black regions represent the donor phase and the acceptor phase, respectively. Since the mixing ratio of P3HT:PCBM is considered to be 1:1, the domain sizes of two phases are assumed to be equal.

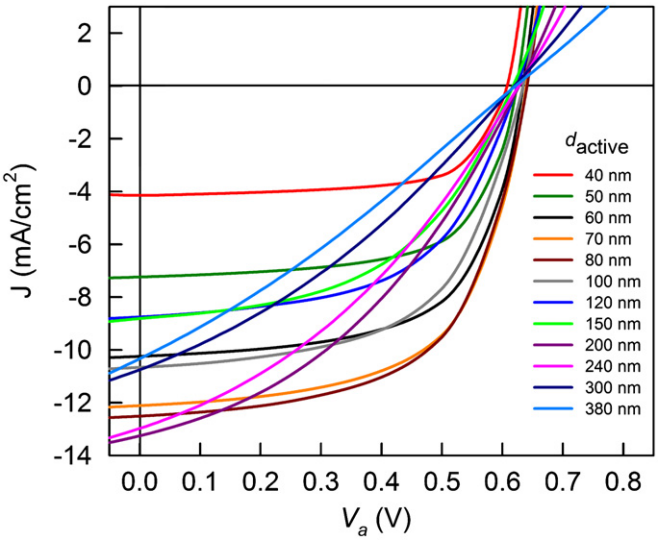

Fig. 4. Simulated $J-V$ curves of devices with different thicknesses of active layer. The domain size l_D of the morphology is 10 nm.

morphology of P3HT/PCBM BHJ, which is intrinsically random. Recently, a simple rectangular 2D model was used as a model morphology for BHJ by Maturova et al. [43]. In their model, the active layer is divided into two regions, namely donor–acceptor mix and acceptor pure phase. They assumed that the dissociation of exciton and the subsequent generation of charges occur homogeneously within the donor–acceptor mixed phase not at the interface between two phases. Therefore, their assumption makes it difficult to establish the relationship between the performance of OPVs and the domain size of morphology.

To describe the dissociation of exciton at the interface more explicitly, the active layer is divided in two regions, the donor- and the acceptor-rich phase. To realistically model the morphology of active layer, we assume that the interface between two phases is sinusoidal rather than the straight line and that the donor and acceptor phases have the same domain size, as shown in Fig. 3. Using the sinusoidal morphology, the thickness of active layer was varied from 40 to 380 nm while the domain size l_D was varied from 4 to 40 nm.

While the applied voltage is changed from -0.1 to 0.8 V, the photocurrent densities of the model devices are calculated by using the drift-diffusion model, where the exciton generation rate was taken from the result of the optical simulation. Fig. 4 shows simulated J–V curves for the devices with the domain size of 10 nm but different thicknesses of the active layer. The open-circuit voltages (V_{OC}) of all the model devices are about 0.6 V regardless of the thickness of the active layer and the domain size (data not shown). This behavior is easily expected because it has been known that V_{OC} depends mostly on the energy levels of the donor and acceptor materials.

Contrary to V_{OC}, the short-circuit current (J_{SC}) of the device changes dramatically with the thickness of the active layer. The thickness dependence of J_{SC}, power conversion efficiency (PCE) and fill factor (FF) are shown in Fig. 5, where the domain size for the model morphology is varied from 4 to 40 nm. The plot of J_{SC} versus thickness shows two maxima at ca. 80 and 220 nm, as shown in Fig. 5(a). Since the number of photons absorbed in the active layer shows an oscillatory nature as the thickness of active layer increases (Fig. 2), the J_{SC} of the model devices also shows oscillatory behavior, because the photocurrent of solar cells depends on the number of photon absorbed in the active layer. However, the photocurrent at 380 nm is not so large as that at 220 nm (Fig. 5(a)), whereas the number of photons absorbed at 380 nm is larger than that at 220 nm (Fig. 2). Lower current density in active layer device can be attributed to the following two reasons: as the thickness of active layer increases, the electric filed inside the active layer decreases at the constant bias voltage. Since the exciton dissociation rate depends on the electric field, the dissociation rate of excitons becomes smaller at lower electric field. Another possible reason for the decrease of J_{SC} in thicker active layer is an increase in the recombination rate. Since a thicker device has longer pathway for charge collection, it is easily expected that the probability for separated charges to recombine increases. Furthermore, due to lower electric field within thicker device under the short-circuit condition, the drift of charge carriers becomes slower and therefore the chance of recombination would be increased. The fraction of recombination events can be evaluated from the ratio of the recombination rate to the dissociation rate under the steady state. Our simulation results show that in the device with $l_D = 10$ nm, 46.2% of dissociated charges are recombined in 380-thick active layer, while 19.5% of dissociated charges are recombined in 220 nm-thick active layer. Considering the different dissociation rates, the net amount of free charge carriers in 220-nm thick active layer are 19.7% larger than in 380-nm thick active layer. This value is close to the difference of the short-circuit current density between two layers (24.5%). Thus, smaller short-circuit current density in thicker device is mainly attributed to an increase of the recombination rate.

The fill factor of model device decreases almost linearly as the thickness of active layer increases (Fig. 5(b)), which is in agreement with previous report [34]. The fill factor is defined by the equation $FF = V_{max}J_{max}/(V_{OC}J_{SC}) \times 100\%$, where V_{max} and J_{max} is the voltage and the current density at the maximum power point on $J-V$ curve, respectively. The electric field at the maximum power point on $J-V$ curve is smaller than that at short-circuit condition, resulting in a lower dissociation rate and a higher recombination rate [49]. The electric field in thicker device becomes also smaller due to the larger distance between the electrodes. Thus the recombination of charge carriers at the maximum power point is more prominent in thicker device, resulting in a low FF. The PCEs of the model devices are calculated from the equation $PCE = (FF) \times V_{OC}J_{SC}/P_{light} \times 100(\%)$, where P_{light} is the incident solar power which is taken to be 100 mW/cm^2 in this study. When the PCE is plotted against the thickness of active layer, as shown in Fig. 5(c), it reveals that the PCE has a maximum at 80 nm thickness. However, unlike J_{SC}, the PCEs at 220 nm

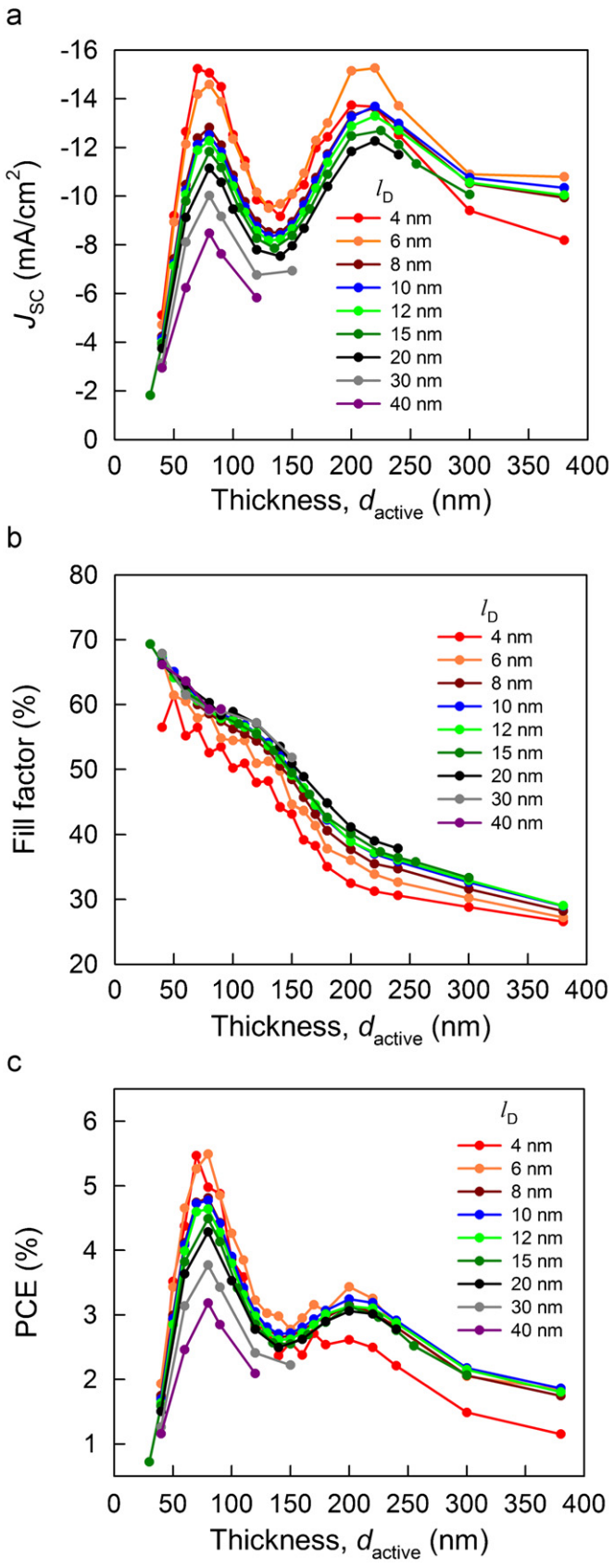

Fig. 5. Plots of (a) J_{SC}, (b) fill factor and (c) PCE as a function of thickness of active layer with different domain size.

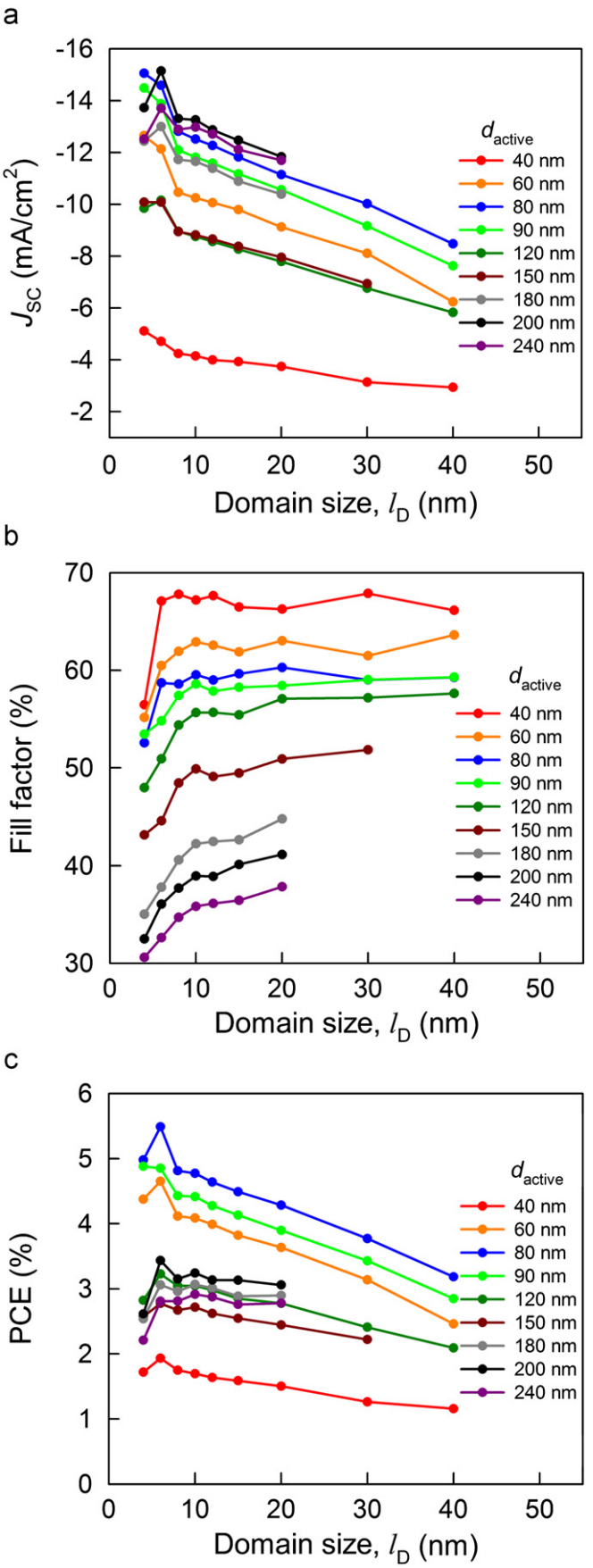

Fig. 6. Plots of (a) J_{SC}, (b) fill factor and (c) PCE as a function of domain size with different thicknesses of active layer.

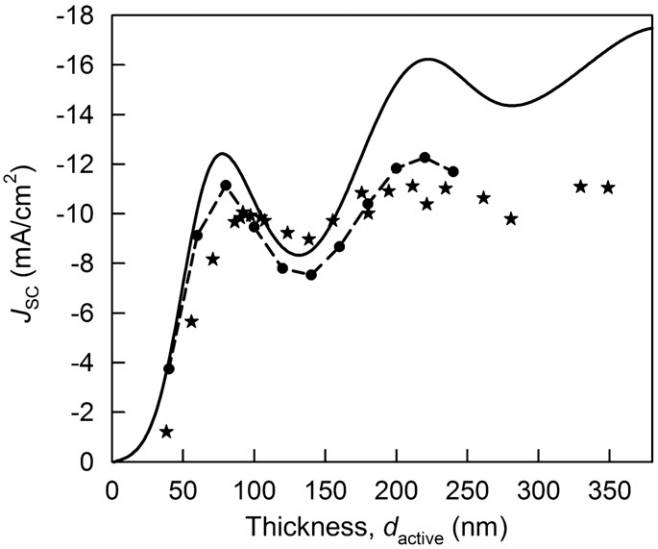

Fig. 7. Comparison of simulated J_{SC} with experimental J_{SC} as a function of thickness of active layer, where l_D=20 nm was used for simulation and experimental data (star) are taken from Ref. [35] and calculated J_{SC}max (solid line) from optical simulation assuming that all absorbed photons contributed to currents. The simulated J_{SC} for domain size of 20 nm is best fit to experimental data.

thickness are much lower than those at 80 nm thickness. This is attributed mainly to lower fill factor of thicker device.

To investigate the effect of domain size (l_D) on the photovoltaic properties, J_{SC}, FF and PCE, are calculated as a function of domain size. When J_{SC}, FF and PCE are plotted against l_D, as shown in Fig. 6, it reveals that both J_{SC} and PCE show a maximum at 6 nm domain size, which is smaller than the exciton diffusion length (8.5 nm) [62], while FF increases and then levels off above 10 nm . As the domain size increases, the interfacial area between donor and acceptor decreases and therefore both the dissociation rate of excitons and the recombination rate decreases, which results in a maximum of J_{SC} and PCE. As mentioned earlier, the fill factor is strongly dependent upon the loss of charges due to recombination at the maximum power point. When the recombination loss is calculated as a function of domain size, it reveals that the recombination loss decreases with increasing the domain size: 29.5%, 20.0%, 16.8%, 14.6%, 13.0% for the domain size of 4, 8, 12, 20, 40 nm, respectively, in the active layer of 120 nm thickness. The increase of fill factor with domain size (Fig. 6(b)) is therefore attributed to the decrease of recombination.

When the calculated J_{SC} values are compared with experimental value [35], as shown in Fig. 7, the calculated values are well consistent with experimental ones, although the thickness of ITO and PEDOT:PSS layer in experiment slightly differs from the values for simulation in this study. Therefore, it is concluded that our simulation properly predicts the photovoltaic properties of solar cell and therefore provides a useful information for optimizing the device parameters.

4. Conclusions

We have investigated the relationship between the device performance of photovoltaic cells and the device parameters such as the thickness of active layer and the domain size in bulk-heterojunction solar cells by using a two-dimensional drift-diffusion model with transfer matrix formalism. When we assume that bulk-heterojunction has sinusoidal morphology, simulation results are in good agreement with experimental data reported by other groups [35]. The results of simulation lead us to conclude that the photocurrent is highly dependent upon the thickness of active layer due to the optical effects and that the optimum domain size is smaller than the exciton diffusion length.

Acknowledgements

The authors thank the Ministry of Education, Science and Technology (MEST), Korea for financial support through the Global Research Laboratory (GRL) program.

References

[1] F.C. Krebs, Fabrication and processing of polymer solar cells: a review of printing and coating techniques, Sol. Energy Mater. Sol. Cells 93 (2009) 394–412.
[2] B. Kippelen, J.L. Bredas, Organic photovoltaics, Energy Environ. Sci. 2 (2009) 251–261.
[3] S. Gunes, H. Neugebauer, N.S. Sariciftci, Conjugated polymer-based organic solar cells, Chem. Rev. 107 (2007) 1324–1338.
[4] I. Gonzalez-Valls, M. Lira-Cantu, Vertically-aligned nanostructures of ZnO for excitonic solar cells: a review, Energy Environ. Sci. 2 (2009) 19–34.
[5] T. Ameri, G. Dennler, C. Lungenschmied, C.J. Brabec, Organic tandem solar cells: a review, Energy Environ. Sci. 2 (2009) 347–363.
[6] M. Helgesen, R. Sondergaard, F.C. Krebs, Advanced materials and processes for polymer solar cell devices, J. Mater. Chem. 20 (2010) 36–60.
[7] V.D. Mihailetchi, L.J.A. Koster, P.W.M. Blom, C. Melzer, B. De Boer, J.K.J. Van Duren, R.A.J. Janssen, Compositional dependence of the performance of poly(p-phenylene vinylene): methanofullerene bulk-heterojunction solar cells, Adv. Funct. Mater. 15 (2005) 795–801.
[8] T. Nishizawa, K. Tajima, K. Hashimoto, The effect of crystallinity in donor groups on the performance of photovoltaic devices based on an oligothiophene–fullerene dyad, Nanotechnology 19 (2008) 424017-1–424017-8.
[9] T. Erb, U. Zhokhavets, G. Gobsch, S. Raleva, B. Stuhn, P. Schilinsky, C. Waldauf, C.J. Brabec, Correlation between structural and optical properties of composite polymer/fullerene films for organic solar cells, Adv. Funct. Mater. 15 (2005) 1193–1196.
[10] G. Li, V. Shrotriya, J.S. Huang, Y. Yao, T. Moriarty, K. Emery, Y. Yang, High-efficiency solution processable polymer photovoltaic cells by self-organization of polymer blends, Nat. Mater. 4 (2005) 864–868.
[11] W.L. Ma, C.Y. Yang, X. Gong, K. Lee, A.J. Heeger, Thermally stable, efficient polymer solar cells with nanoscale control of the interpenetrating network morphology, Adv. Funct. Mater. 15 (2005) 1617–1622.
[12] Y. Kim, S. Cook, S.M. Tuladhar, S.A. Choulis, J. Nelson, J.R. Durrant, D.D.C. Bradley, M. Giles, I. Mcculloch, C.S. Ha, M. Ree, A strong regioregularity effect in self-organizing conjugated polymer films and high-efficiency polythiophene:fullerene solar cells, Nat. Mater. 5 (2006) 197–203.
[13] M. Reyes-Reyes, K. Kim, D.L. Carroll, High-efficiency photovoltaic devices based on annealed poly(3-hexylthiophene) and 1-(3-methoxycarbonyl)-propyl-1-phenyl-(6,6)C-61 blends, Appl. Phys. Lett. 87 (2005) 083506-1–083506-3.
[14] G. Yu, A.J. Heeger, Charge separation and photovoltaic conversion in polymer composites with internal dornor–acceptor heterojunctions, J. Appl. Phys. 78 (1995) 4510–4515.
[15] J.Y. Kim, K. Lee, N.E. Coates, D. Moses, T.Q. Nguyen, M. Dante, A.J. Heeger, Efficient tandem polymer solar cells fabricated by all-solution processing, Science 317 (2007) 222–225.
[16] Y. Yao, J.H. Hou, Z. Xu, G. Li, Y. Yang, Effect of solvent mixture on the nanoscale phase separation in polymer solar cells, Adv. Funct. Mater. 18 (2008) 1783–1789.
[17] J.Y. Kim, S.H. Kim, H.H. Lee, K. Lee, W.L. Ma, X. Gong, A.J. Heeger, New architecture for high-efficiency polymer photovoltaic cells using solution-based titanium oxide as an optical spacer, Adv. Mater. 18 (2006) 572–576.
[18] J. Gilot, I. Barbu, M.M. Wienk, R.A.J. Janssen, The use of ZnO as optical spacer in polymer solar cells: theoretical and experimental study, Appl. Phys. Lett. 91 (2007) 113520-1–113520-3.
[19] J.U. Lee, A. Cirpan, T. Emrick, T.P. Russell, W.H. Jo, Synthesis and photophysical property of well-defined donor–acceptor diblock copolymer based on regioregular poly(3-hexylthiophene) and fullerene, J. Mater. Chem. 19 (2009) 1483–1489.
[20] J.U. Lee, J.W. Jung, T. Emrick, T.P. Russell, W.H. Jo, Morphology control of a polythiophene–fullerene bulk heterojunction for enhancement of the high-temperature stability of solar cell performance by a new donor–acceptor diblock copolymer, Nanotechnology 21 (2010) 105201-1–105201-9.
[21] M.C. Scharber, D. Wuhlbacher, M. Koppe, P. Denk, C. Waldauf, A.J. Heeger, C.L. Brabec, Design rules for donors in bulk-heterojunction solar cells—towards 10% energy-conversion efficiency, Adv. Mater. 18 (2006) 789–794.
[22] G. Dennler, M.C. Scharber, T. Ameri, P. Denk, K. Forberich, C. Waldauf, C.J. Brabec, Design rules for donors in bulk-heterojunction tandem solar cells-towards 15% energy-conversion efficiency, Adv. Mater. 20 (2008) 579–583.

[23] M. Al-Ibrahim, H.K. Roth, U. Zhokhavets, G. Gobsch, S. Sensfuss, Flexible large area polymer solar cells based on poly(3-hexylthiophene)/fullerene, Sol. Energy Mater. Sol. Cells 85 (2005) 13–20.
[24] F.C. Krebs, M. Jorgensen, K. Norrman, O. Hagemann, J. Alstrup, T.D. Nielsen, J. Fyenbo, K. Larsen, J. Kristensen, A complete process for production of flexible large area polymer solar cells entirely using screen printing—first public demonstration, Sol. Energy Mater. Sol. Cells 93 (2009) 422–441.
[25] F.C. Krebs, J. Alstrup, H. Spanggaard, K. Larsen, E. Kold, Production of large-area polymer solar cells by industrial silk screen printing, lifetime considerations and lamination with polyethyleneterephthalate, Sol. Energy Mater. Sol. Cells 83 (2004) 293–300.
[26] M. Jorgensen, K. Norrman, F.C. Krebs, Stability/degradation of polymer solar cells, Sol. Energy Mater. Sol. Cells 92 (2008) 686–714.
[27] F.C. Krebs, H. Spanggaard, Significant improvement of polymer solar cell stability, Chem. Mater. 17 (2005) 5235–5237.
[28] J.M. Nunzi, Organic photovoltaic materials and devices, C. R. Phys. 3 (2002) 523–542.
[29] J. Jo, S.I. Na, S.S. Kim, T.W. Lee, Y. Chung, S.J. Kang, D. Vak, D.Y. Kim, Three-dimensional bulk heterojunction morphology for achieving high internal quantum efficiency in polymer solar cells, Adv. Func. Mater. 19 (2009) 2398–2406.
[30] S.E. Shaheen, C.J. Brabec, N.S. Sariciftci, F. Padinger, T. Fromherz, J.C. Hummelen, 2.5% efficient organic plastic solar cells, Appl. Phys. Lett. 78 (2001) 841–843.
[31] S. Miyanishi, K. Tajima, K. Hashimoto, Morphological stabilization of polymer photovoltaic cells by using cross-linkable poly(3-(5-hexenyl)thiophene), Macromolecules 42 (2009) 1610–1618.
[32] P.K. Watkins, A.B. Walker, G.L.B. Verschoor, Dynamical Monte Carlo modelling of organic solar cells: the dependence of internal quantum efficiency on morphology, Nano Lett. 5 (2005) 1814–1818.
[33] L.A.A. Pettersson, L.S. Roman, O. Inganas, Modeling photocurrent action spectra of photovoltaic devices based on organic thin films, J. Appl. Phys. 86 (1999) 487–496.
[34] D.W. Sievers, V. Shrotriya, Y. Yang, Modeling optical effects and thickness dependent current in polymer bulk-heterojunction solar cells, J. Appl. Phys. 100 (2006) 114509-1–114509-7.
[35] A.J. Moule, K. Meerholz, Minimizing optical losses in bulk heterojunction polymer solar cells, Appl. Phys. B: Lasers Opt. 86 (2007) 721–727.
[36] T. Ameri, G. Dennler, C. Waldauf, P. Denk, K. Forberich, M.C. Scharber, C.J. Brabec, K. Hingerl, Realization, characterization and optical modeling of inverted bulk-heterojunction organic solar cells, J. Appl. Phys. 103 (2008) 084506-1–084506-6.
[37] G.A. Buxton, N. Clarke, Predicting structure and property relations in polymeric photovoltaic devices, Phys. Rev. B 74 (2006) 085207-1–085207-5.
[38] G.A. Buxton, N. Clarke, Computer simulation of polymer solar cells, Modelling Simulation Mater. Sci. Eng. 15 (2007) 13–26.
[39] G. Dennler, K. Forberich, M.C. Scharber, C.J. Brabec, I. Tomis, K. Hingerl, T. Fromherz, Angle dependence of external and internal quantum efficiencies in bulk-heterojunction organic solar cells, J. Appl. Phys. 102 (2007) 054516-1–054516-7.
[40] S. Lacic, O. Inganas, Modeling electrical transport in blend heterojunction organic solar cells, J. Appl. Phys. 97 (2005) 124901-1–124901-7.
[41] B. Lei, Y. Yao, A. Kumar, Y. Yang, V. Ozolins, Quantifying the relation between the morphology and performance of polymer solar cells using Monte Carlo simulations, J. Appl. Phys. 104 (2008) 024504-1–024504-6.
[42] R.A. Marsh, C. Groves, N.C. Greenham, A microscopic model for the behavior of nanostructured organic photovoltaic devices, J. Appl. Phys. 101 (2007) 083509-1–083509-7.
[43] K. Maturova, S.S. Van Bavel, M.M. Wienk, R.A.J. Janssen, M. Kemerink, Morphological device model for organic bulk heterojunction solar cells, Nano Lett. 9 (2009) 3032–3037.
[44] B. Ruhstaller, S.A. Carter, S. Barth, H. Riel, W. Riess, J.C. Scott, Transient and steady-state behavior of space charges in multilayer organic light-emitting diodes, J. Appl. Phys. 89 (2001) 4575–4586.
[45] J.C. Scott, G.G. Malliaras, Charge injection and recombination at the metal-organic interface, Chem. Phys. Lett. 299 (1999) 115–119.
[46] S. Selberherr, Analysis and Simulation of Semiconductor Devices, first ed., Springer-Verlag, Wien, 1984.
[47] P.K. Watkins, A.B. Walker, G.L.B. Verschoor, Dynamical Monte Carlo modelling of organic solar cells: the dependence of internal quantum efficiency on morphology, Nano Lett. 5 (2005) 1814–1818.
[48] J.A. Barker, C.M. Ramsdale, N.C. Greenham, Modeling the current–voltage characteristics of bilayer polymer photovoltaic devices, Phys. Rev. B 67 (2003) 075205-1–075205-9.
[49] L.J.A. Koster, E.C.P. Smits, V.D. Mihailetchi, P.W.M. Blom, Device model for the operation of polymer/fullerene bulk heterojunction solar cells, Phys. Rev. B 72 (2005) 085205-1–085205-9.
[50] H. Hoppe, N.S. Sariciftci, Morphology of polymer/fullerene bulk heterojunction solar cells, J. Mater. Chem. 16 (2006) 45–61.
[51] F. Monestier, J.J. Simon, P. Torchio, L. Escoubas, F. Florya, S. Bailly, R. De Bettignies, S. Guillerez, C. Defranoux, Modeling the short-circuit current density of polymer solar cells based on P3HT:PCBM blend, Sol. Energy Mater. Sol. Cells 91 (2007) 405–410.
[52] A.J. Moule, J.B. Bonekamp, K. Meerholz, The effect of active layer thickness and composition on the performance of bulk-heterojunction solar cells, J. Appl. Phys. 100 (2006) 094503-1–094503-7.
[53] R.M.A. Azzam, N.M. Bashara, Ellipsometry and Polarized Light, first ed., North-Holland, Amsterdam, 1977.
[54] D.X. Zhu, W.D. Shen, H. Ye, X. Liu, H.Y. Zhen, Determination of the optical constants of polymer light-emitting diode films from single reflection measurements, J. Phys. D: Appl. Phys. 41 (2008) 235104-1–235104-5.
[55] M. Bass, Handbook of Optics, second ed., McGraw-Hill, New York, 1995.
[56] M. Losurdo, M. Giangregorio, P. Capezzuto, G. Bruno, R. De Rosa, F. Roca, C. Summonte, J. Pla, R. Rizzoli, Parametrization of optical properties of indium–tin-oxide thin films by spectroscopic ellipsometry: substrate interfacial reactivity, J. Vac. Sci. Technol. A 20 (2002) 37–42.
[57] D.Y. Smith, E. Shiles, M. Inokuti, The optical properties of metallic aluminum, in: E.D. Palik (Ed.), Handbook of Optical Constants of Solids, Academic Press, San Diego, 1998, pp. 395–401.
[58] C.L. Braun, Electric field assisted dissociation of charge transfer states as a mechanism of photocarrier production, J. Chem. Phys. 80 (1984) 4157–4161.
[59] T.E. Goliber, J.H. Perlstein, Analysis of photogeneration in a doped polymer system in terms of a kinetic-model for electric-field-assisted dissociation of charge-transfer states, J. Chem. Phys. 80 (1984) 4162–4167.
[60] D.L. Scharfetter, H.K. Gummel, Large-signal analysis of a silicon read diode oscillator, IEEE Trans. Electron Dev. 16 (1969) 64–77.
[61] ASTM, in: ASTM G173-03e1 Standard Tables for Reference Solar Spectral Irradiances: Direct Normal and Hemispherical on 37 Tilted Surface, American Society for Testing and Materials, 2003, pp. 1–20.
[62] P.E. Shaw, A. Ruseckas, I.D.W. Samuel, Exciton diffusion measurements in poly(3-hexylthiophene), Adv. Mater. 20 (2008) 3516–3520.
[63] C. Goh, R.J. Kline, M.D. Mcgehee, E.N. Kadnikova, J.M.J. Frechet, Molecular-weight-dependent mobilities in regioregular poly(3-hexyl-thiophene) diodes, Appl. Phys. Lett. 86 (2005) 122110-1–122110-3.
[64] S.K.M. Jonsson, W.R. Salaneck, M. Fahman, Photoemission of Alq(3) and C-60 films on Al and LIF/Al substrates, J. Appl. Phys. 98 (2005) 014901-1–014901-7.
[65] P. Kumar, S.C. Jain, V. Kumar, S. Chand, R.P. Tandon, Effect of illumination on the space charge limited current in organic bulk heterojunction diodes, Appl. Phys. A: Mater. Sci. Process 94 (2009) 281–286.